remote sensing

MDPI

Article

Unveiling Temperature Patterns in Tree Canopies across Diverse Heights and Types

Riyaaz Uddien Shaik [1,*,†], Sriram Babu Jallu [2,†] and Katarina Doctor [3]

[1] School of Aerospace Engineering, Sapienza University of Rome, 00138 Rome, Italy
[2] Wageningen University & Research, 6700 HB Wageningen, The Netherlands
[3] Naval Research Laboratory, Navy Center for Applied Research in Artificial Intelligence, Washington, DC 20375, USA
* Correspondence: riyaaz.shaik@uniroma1.it
† These authors contributed equally to this work.

Abstract: Forests are some of the major ecosystems that help in mitigating the effects of climate change. Understanding the relation between the surface temperatures of different vegetation and trees and their heights is very crucial in understanding events such as wildfires. In this work, relationships between tree canopy temperature and canopy height with respect to vegetation types were extracted. The southern part of Sardinia Island, which has dense forests and is often affected by wildfires, was selected as the region of interest. PRISMA hyperspectral imagery has been used to map all the available vegetation types in the region of interest using the support vector machine classifier with an accuracy of >80% for all classes. The Global Ecosystem Dynamics Investigation's (GEDI) L2A Raster Canopy Top Height product provides canopy height measurements in spatially discrete footprints, and to overcome this issue of discontinuous sampling, Random Forest Regression was used on Sentinel-1 SAR data, Sentinel-2 multispectral data, and the Shuttle Radar Topography Mission (SRTM) digital elevation model (DEM) to estimate the canopy heights of various vegetation classes, with a root mean squared error (RMSE) value of 2.9176 m and a coefficient of determination (R^2) value of 0.791. Finally, the Moderate Resolution Imaging Spectroradiometer (MODIS) Land Surface Temperature (LST) and emissivity product provides ground surface temperature regardless of land use and land cover (LULC) types. LST measurements over tree canopies are considered as the tree canopy temperature. We estimated the relationship between the canopy temperature of five vegetation types (evergreen oak, olive, juniper, silicicole, riparian trees) and the corresponding canopy heights and vegetation types. The resulting scatter plots showed that lower tree canopy temperatures correspond with higher tree canopies with a correlation coefficient in the range of −0.4 to −0.5 for distinct types of vegetation.

Keywords: canopy heights; hyperspectral; lidar; multispectral; synthetic aperture radar; tree canopy temperature

Citation: Shaik, R.U.; Jallu, S.B.; Doctor, K. Unveiling Temperature Patterns in Tree Canopies across Diverse Heights and Types. *Remote Sens.* **2023**, *15*, 2080. https://doi.org/10.3390/rs15082080

Academic Editors: Chung-Te Chang and Junhu Dai

Received: 5 March 2023
Revised: 3 April 2023
Accepted: 4 April 2023
Published: 14 April 2023

1. Introduction

Forests perform some of the crucial ecological functions that help support the climate of the Earth as well mitigate the negative effects of climate change, as they act as natural carbon sinks and provide a variety of biodiversity. Maintaining the forest's ecosystem is highly crucial (https://sustainabletravel.org, accessed on 20 January 2023) [1]. To achieve that, understanding the relationship between the spatial features of forests is especially important, some of which include canopy cover, height, biomass, and surface temperature [1]. The biophysical feedback of the forest canopy height changes on the land surface temperature (LST) also has been investigated, and it has been concluded that forests with taller trees evaporate more water into the atmosphere and absorb more heat from the surrounding environment than forests with shorter trees do, leading to a net cooling effect [1,2].

LST is one of the principal factors in supporting a balance of surface energy [2–4]. This plays a vital role in one of the most significant effects, known as urban heat islands. It is a phenomenon that is caused by the removal of natural vegetation and the use of low-albedo construction materials and roads, as well as by heat produced by human activity, such as the heat from cars, air conditioners, industries, refrigerants, aerosols, and gas stations [5,6]. Another impactful use of LST is associated with its applications in studying wildfires [7–9]. Using the differenced normalized burn ratio (dNBR) in monitoring the severity of burned zones, the statistical difference between the LST and the normalized difference vegetation index (NDVI) was observed in the burn severity categories, which showed substantial changes in LST in the zones of higher fire severity [10]. The relationship between LST and various landscape features, such as the NDVI, which shows vegetation health, and the normalized difference water index (NDWI), which shows the water content of vegetation from multi- or hyperspectral imagery, has also been examined [11].

Our literature survey showed that understanding the canopy temperature is important and why is it important is explained in Box 1.

Box 1. Why Is Understanding the Relation Between Tree Canopy Temperature and Canopy Height Important?

Monitoring a canopy's height and its temperature changes is of immense importance, just as much as the relationship between them. These changes are caused by various natural and anthropogenic processes, such as deforestation, afforestation, drought stress, wildfires [12], etc. Canopy height and forest structure changes result in significant changes in biophysical properties, such as surface albedo, which directly affects the influx of net radiation and has an impact on surface temperature [13]. Quite a few studies have been conducted exploring the importance of canopy surface temperature. Canopy temperature can be a direct measure for the health of urban trees [14]. Many studies have been conducted acknowledging the importance of the relationship between wildfires and surface temperatures [15,16]. In addition to forests, studies have also been conducted to monitor the changes in trees and distinct types of vegetation in urban areas and the consequences of these changes in terms of urban heat islands [15,16]. There are a variety of issues interlinked with the increase in surface temperatures; for example, trend analyses of forest fire hot spots were carried out for the western Himalyians to check their relationship with LST. The results showed that an increase in mean LST over months led to an increase in the number of overall forest fires [17]. Understanding the patterns of soil moisture and LST has also contributed toward predicting the extent of a wildfire event [18]. Increases in the temperature of a forest lead to the drying up of soil moisture, which, in turn, causes the trees and vegetation to become combustible and eventually gives rise to wildfires. Though wildfires are part of nature, the prevention and management of wildfires is important [19]. Therefore, understanding the relationship between forest canopy height and canopy temperature helps to better understand the local forest climate.

Understanding variation of canopy temperature is important mainly for applications such as wildfire management [17] and vegetation health management [14]. For instance, a trend analysis of forest fire hot spots was performed for the western Himalayas to check their relationship with LST. The results showed that an increase in mean LST over months led to an increase in the number of overall forest fires [17]. Another study showed that canopy temperature can be a direct measure of the health of urban trees [14]. Remotely sensed LST measurements over the trees are based on the principle that the spectral radiance reflected in the thermal infrared bands is from the tree canopy instead of the ground surface beneath the tree. Therefore, remotely sensed LST measurements over trees can be considered as estimated tree canopy temperature and can be used for understanding the spatial pattern of canopy temperatures. In our study, we used MODIS LST and emissivity product (MOD 21) to extract tree canopy temperatures.

The biophysical and biogeochemical processes of forests, such as albedo, evapotranspiration, canopy roughness, water cycle, and carbon cycle, help in mitigating the effects of climate change [20–22]. In terms of spatial information, some of these attributes are the most crucial information for effectively and sustainably preserving forest resources and for making informed decisions about supporting biodiversity [23,24]. The demand for

spatially explicit data of forest attributes has grown tremendously, and is sought by local, national, and global agencies. For example, forest biomass has been recognized by the Global Climate Observing System as an essential environmental variable [25]. Moreover, these agencies need these forest attributes at high spatial resolutions for proper monitoring of the changes occurring in the forest ecosystem. Canopy height has been shown to be the top predictor for forest mortality during extreme drought conditions. Larger trees die at a rate twice as fast as smaller ones, and younger trees had higher growth reductions during droughts. However, forests with younger canopies recover more quickly from drought [26–28].

Light detection and ranging (lidar) technology have revolutionized the collection of spatial information of forests, including canopy heights. This technology can be adopted on various platforms such as on the ground, on unmanned aerial vehicles, or even in satellite-based imaging [29]. At present, GEDI is NASA's first spaceborne, full-waveform lidar that is specifically designed to measure ecosystem structure by providing vertical profiles of forest canopies. After its launch, recent studies have been appropriately making full use of its data, such as in mapping the canopy forest with the integration of GEDI and Landsat datasets [30], conducting plant health assessments using spatial canopy features such as canopy height and diameter at breast height [31], using spatial features of forests in wildfire management [32], and many more. Unlike gridded imagery from optical satellites such as Landsat-8, Sentinel-2, etc., GEDI is a sampling instrument that can record height measurements in spatially discrete ~25 m diameter footprints, where interstitial areas remain unsampled between footprints (60 m along-track) and between transects (600 m across-track) [33]. Though this sensor has near-global coverage, it comes at the expense of unsampled gaps, for example, the inability of near-infrared lidar to penetrate clouds and the undersampling of some regions owing to limitations of the International Space Station's orbital geometry [34]. Due to these limitations, researchers around the world are developing approaches to estimate canopy heights using other available continuous gridded imagery. Some of the instances reported on estimating continuous forest canopy heights using GEDI data as a proxy for in situ data are as follows: A paper reported using different machine learning algorithms with airborne laser data, spaceborne radar data, and GEDI data as a proxy for in situ data [30] to estimate forest canopy heights. Lang et al. [35] reported using a convolution neural network (CNN) model with Sentinel-2 data to estimate vegetation heights. A study used the neural network-guided interpolation (NNGI) method to integrate the GEDI, ICESat-2 ATLAS, and Sentinel-2 optical images to map forest canopy heights [36]. Based on these instances, the GEDI canopy height product is a reliable and suitable ground truth for predicting canopy heights. We understood from our literature survey that radio detection and ranging (radar) data, optical data, and elevation and slope data had major impacts in estimating canopy heights, so we trained a random forest regression model using Sentinel-1 synthetic aperture radar (SAR) data, Sentinel-2 multispectral data, and SRTM elevation and slope data as independent variables and canopy height measurements from GEDI as the dependent variable to continuously predict canopy heights for our region of interest. Apart from canopy heights, on the topic of spatial features of forests and forest ecosystem management, LULC maps are a crucial part of these activities.

We are interested in analyzing the spatial distribution of canopy temperature across various types of vegetation in our study area; therefore, a land use and land cover mapping has been conducted. LULC mapping has been one of the most researched topics in remote sensing and geographic information sciences. The significance of the knowledge of the land cover of a certain location is unmatched when performing change analyses, in urban planning, thematic mapping, agriculture, deforestation, or reforestation, and in determining the relationship of land use to climate change [22,37]. This spatial information helps to better understand the use of land. It is also used for retrieving various biophysical variables, such as vegetation indices about vegetation health, water content, and carbon content. The biophysical effects of the LULC changes have also been extensively studied using satellite imagery [38]. Even the changes in the structure of the forests lead to significant

changes in some important biophysical properties, such as a change in the surface energy and albedo, eventually leading to a change in the surface temperature [39–41]. Offline simulations have been performed to see the impact of the structural changes of a forest on the surface temperature and showed a decrease in both daytime and nighttime LST over regions of grassland to forest transition, corresponding to average values of 0.44 and 0.20 K, respectively. Authors have reported that this is predominantly controlled by changes in evapotranspiration [42]. Various supervised and unsupervised image-classifying methodologies have been used to classify land cover, such as image segmentation, artificial neural network-based classification, and object-based classification [43,44]. Many studies [45] have reported that hyperspectral imagery is prominent in remote sensing, with its wide range of applications in precision agriculture and environmental modelling [46], and is able to map LULC types with comparatively better accuracy [47]. PRISMA, a spaceborne hyperspectral satellite of the Italian Space Agency, has proven suitable for vegetation mapping [48], and it is considered in our study for mapping different vegetation types.

In this work, we tried to understand the spatial pattern of forest canopy temperatures for varying canopy heights and different tree types for the southern part of Sardinian Island that constitutes the Monte-Arcosu Forest. This effort requires three different maps, viz., a tree canopy temperature map, a canopy height map, and an LULC map for the region of interest. We generated these three maps using different sources and methods as follows: Firstly, a random forest regression model was trained using Sentinel-1 SAR data, Sentinel-2 multispectral data, and SRTM elevation and slope data as independent variables and canopy height measurements from the GEDI canopy height product as the dependent variable. Secondly, we classified LULC types for the same area using PRISMA hyperspectral imagery. Finally, we extracted tree canopy temperatures using the MODIS LST and emissivity product. Then, we generated scatter plots for varying canopy heights and vegetation types to examine the relationship between them. This paper is structured as follows: Section 1 introduces all the topics that the paper tries to deal with. Section 2 describes the area of interest. Section 3 talks about the various stages of the research and methodologies used at each stage. Finally, Section 4 concludes with the results obtained and the inferences that were derived from them.

2. Study Area and Data Used

2.1. Study Area

Sardinia is one of the largest Italian islands in the Mediterranean Sea, with the largest forest cover. Sardinia is one of the regions that is most affected by the forest fires during summers. Reports show that the region had a total of 1,008 wildfires annually in the past decade, and that accounts for 20% of the total over the entire nation of Italy (https://data.europa.eu/doi/10.2760/059331, accessed on 20 January 2023). This was the primary reason for choosing a densely forested region as our study area for this project, as shown in Figure 1. The average temperature on the island ranges from 10 °C in winter (January/February) to 24–25 °C in summer (July/August); it has rainy winters and hot, sunny summers, and it has winds ranging from 0.3 mph to 11.5 mph. Much research has been conducted investigating and elucidating the spatial extents and patterns of the forest fires, along with a few studies focusing on the simulations of the events [49].

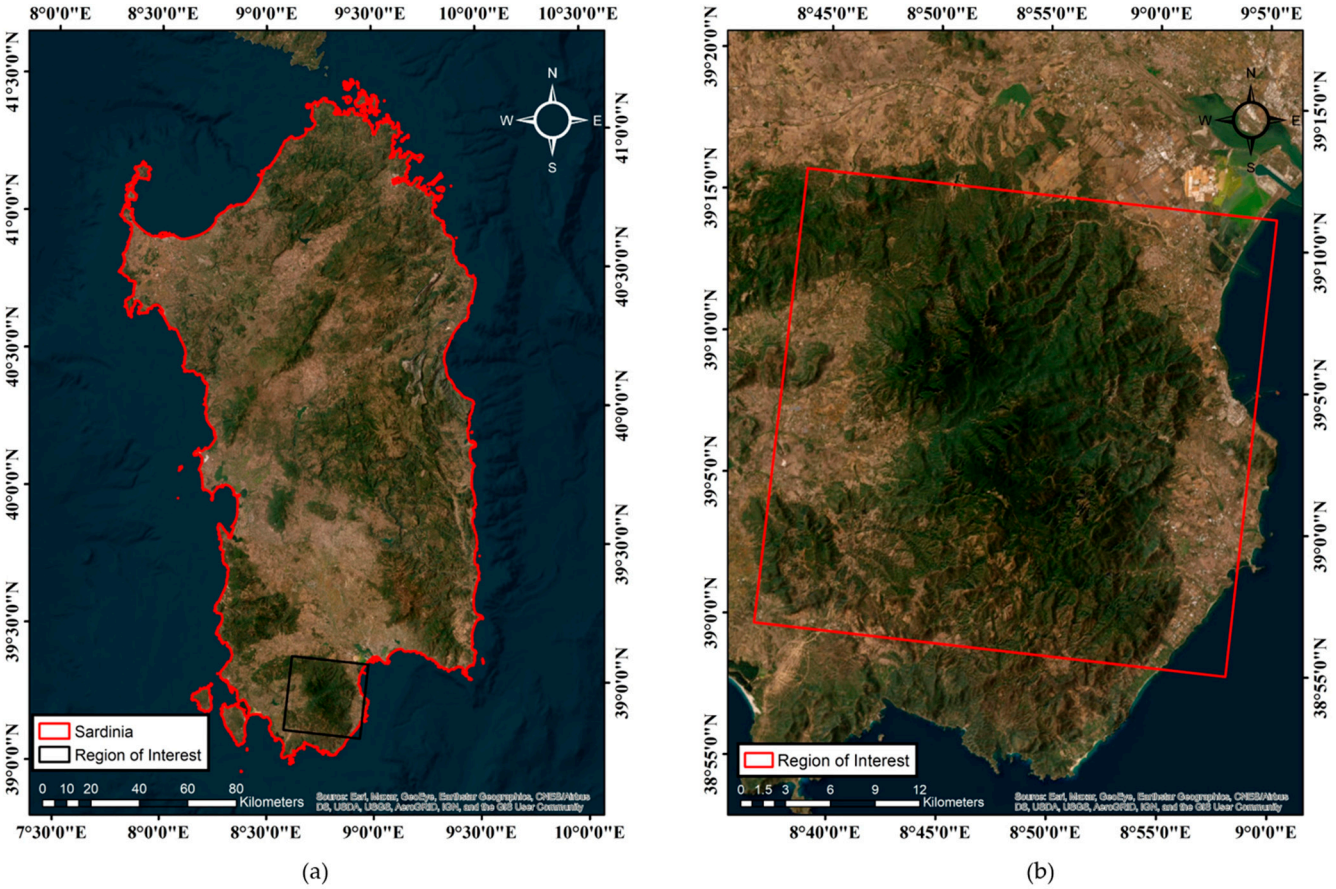

Figure 1. (**a**) Sardinia Island. (**b**) The region of interest is a forested area of 900 square km.

2.2. Remote Sensing Datasets

As explained in the previous section, we utilized freely available remote-sensing datasets for mapping canopy heights, LULC types, and canopy temperatures, as shown in Table 1. To estimate canopy heights, data from Sentinel-1 SAR, Sentinel-2 multispectral, and SRTM elevation and slope products were used as independent variables and canopy height measurements from GEDI's 98th percentile of the relative height (RH98) product was used as the dependent variable to train the random forest regression model. For classification of LULC types, PRISMA hyperspectral imagery, available for free upon registration on prisma.asi.it (accessed on 1 October 2022), has been used in our study. This hyperspectral sensor was launched in 2019 by the Italian Space Agency and captures images in narrow, contiguous, spectral bands having a spectral resolution of ~12 nm and provides images in both VNIR and SWIR wavelength regions, as shown in Table 1. Tree canopy temperatures were extracted over the regions of interest using the MODIS LST and emissivity product that provides daily land surface temperatures as depicted in Table 1.

2.3. Reference Datasets

The current work uses the help of multiple maps, namely, (i) the Nature System Map of Sardinia, which was accessed through the Sardinia Geoportal, (ii) the CORINE Land Cover (CLC) map (2018), and (iii) grassland maps that were obtained through the Copernicus Land Monitoring Services, as reference data for LULC mapping. The Nature System map had an overall accuracy of 85% [50,51]. The CLC map had an overall coverage of 5.8 Mkm^2, and validation studies have shown it to have an overall accuracy of 85% [52]. The grasslands maps helped in identifying the presence and absence of grasslands. These three maps were used for cross-checking the corresponding pixels of trees, grasslands, and shrubs.

Table 1. Remote-Sensing Datasets Utilized in This Study.

Data Type	Spectral Bands	Spatial Resolution (m)	Time Period
PRISMA Hyperspectral Imagery	234 bands (visible infrared and short-wave infrared region)	30	October 2021
Sentinel-1	S1_GRD Product (Interferometric Wide Swath Mode)— VV and VH Polarization	10	August 2021 to October 2021
Sentinel-2	B2 (blue) B3 (green) B4 (red) B5 (near infrared) B6 (near infrared) B7 (near infrared) B8 (near infrared) B11 (short wave infrared) B12 (short wave infrared)	10 10 10 20 20 20 10 20 20	August 2021 to October 2021
SRTM	Digital Elevation Map (SRTMGL1_003)	30	-
GEDI	GEDI's Level 2A Geolocated Elevation and Height Metrics Product	25	April 2019 to October 2021
MODIS	MODIS/Aqua Land Surface Temperature/Emissivity Daily L3 Global Grid	1000	October 2021

3. Methodology

This section describes the methodology implemented to extract canopy temperatures for varying canopy heights and vegetation types. The methodology is summarized in Figure 2 in three stages: (i) canopy height estimation, (ii) land use, land cover (LULC) mapping, and (iii) extraction of canopy temperatures.

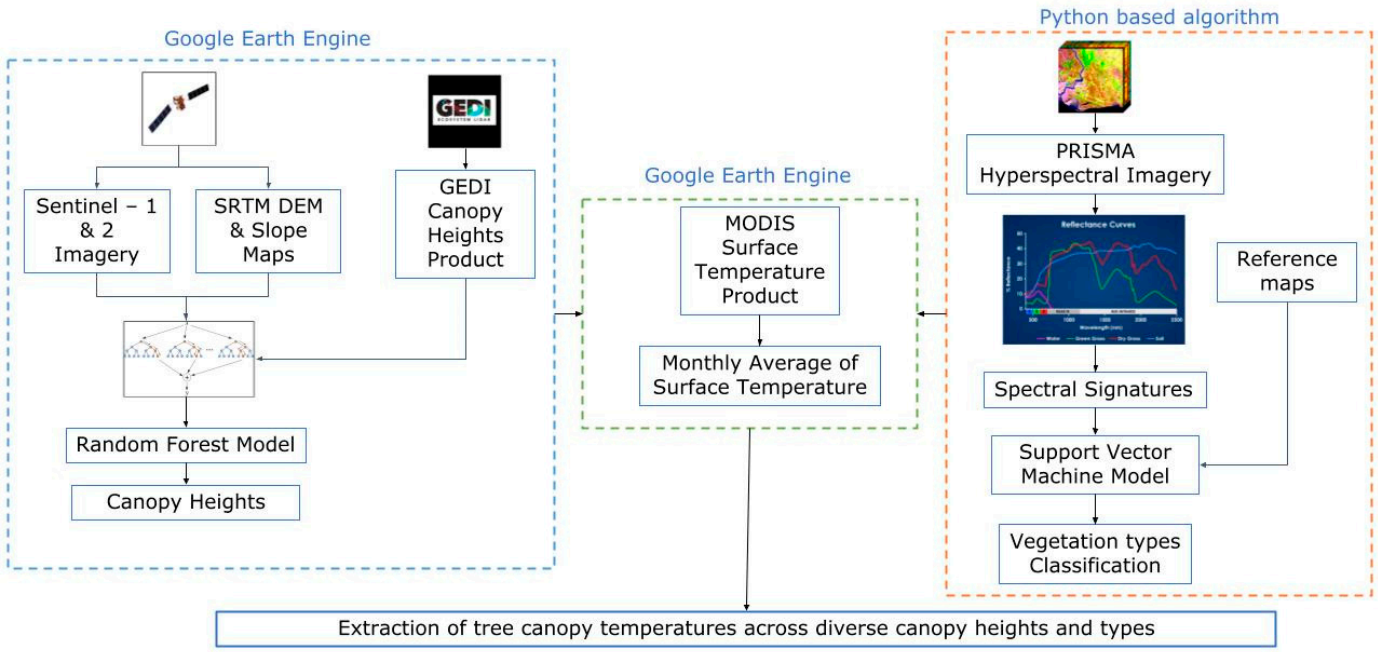

Figure 2. Concept flow chart of canopy height estimation, canopy temperature extraction, and vegetation mapping.

The ability to seamlessly retrieve the data in the Google Earth Engine (GEE) is unmatched, and various packages are available to further enhance its ability for modelling. In our study, canopy height estimation and tree canopy temperature mapping were performed on the GEE cloud computing platform, whereas LULC mapping, with a focus on vegetation classification, was performed with the open access software Python 3.10. A detailed description of the procedure to extract tree canopy temperatures for different canopy heights and tree types is provided in the following subsections.

3.1. Canopy Height Estimation Using GEDI's Canopy Height Product

We selected random forest regression models from Google Earth Engine to predict the canopy heights over a specific region of Sardinia Island. Independent variables of the training dataset include Sentinel-1 GRD product's VV and VH polarization bands, Sentinel-2 sensor's B2 (492 nm) to B8 (892 nm) and B11 (1614 nm) and B12 (2202 nm) bands, and SRTM product's (elevation and slope) maps over a 3-month period (August 2021 to October 2021). The dependent variable in the training dataset is canopy height measurements from the GEDI's RH98 product. An interquartile range (IQR) was computed for the Sentinel-1 GRD images, considering that is where most of the values are present. Sentinel-2 optical bands were collected and a mask was used to remove the cloud cover. The European Space Agency's (ESA) land cover map was used as a reference to collect the entire forest cover over the region. All these bands were then made into a stack for sample collection. In total, a dataset of 15,000 samples was made that was further divided into training (70%), testing (10%), and validation (20%) datasets. The model parameters (variablesPerSplit, minLeafPopulation, bagFraction, maxNodes, and seed) were taken as default values on GEE, and a range of the number of trees (from 10 to 100) (numberOfTrees) was selected to find the optimum result. The variables for the model were chosen randomly, and the final canopy heights were then predicted by calculating the average of the prediction of all the trees. Variable importance has also been calculated to figure out the most important variable that would be helpful in predicting the results. The accuracy of the regression model was estimated by calculating the RMSE and coefficient of determination (R^2) values. The optimization parameters were changed until the highest accuracy of the model was obtained. Figure 3 shows the flow of canopy heights estimation algorithm.

3.2. LULC Classification Using PRISMA Hyperspectral Imagery

Classifying land-use and land-cover types has benefited from the use of hyperspectral imagery. We considered the PRISMA Level 2C product, which is atmospherically corrected and has less than 5% cloud coverage. The PRISMAread tool, developed by the National Research Council of Italy on R software, was used for georeferencing. This tool imports the he5 format files with latitude and longitude information and converts them into GeoTiff or ENVI format files. We used the land cover map included in the PRISMA L1 product to initially differentiate between vegetated and nonvegetated pixels. One of the important preprocessing steps involved in hyperspectral data processing is removing noisy bands, which we performed in MATLAB, excluding bands that have 20% noise. After completing these preprocessing steps, we extracted spectral signatures to train the classification machine learning model using three maps, viz., a grassland map, a nature system map, and a Corine land cover map as ground truth. These maps were collected from the Sardinia Geoportal and the Copernicus Land Monitoring Services Portal. A flowchart of the classification process is shown in Figure 4.

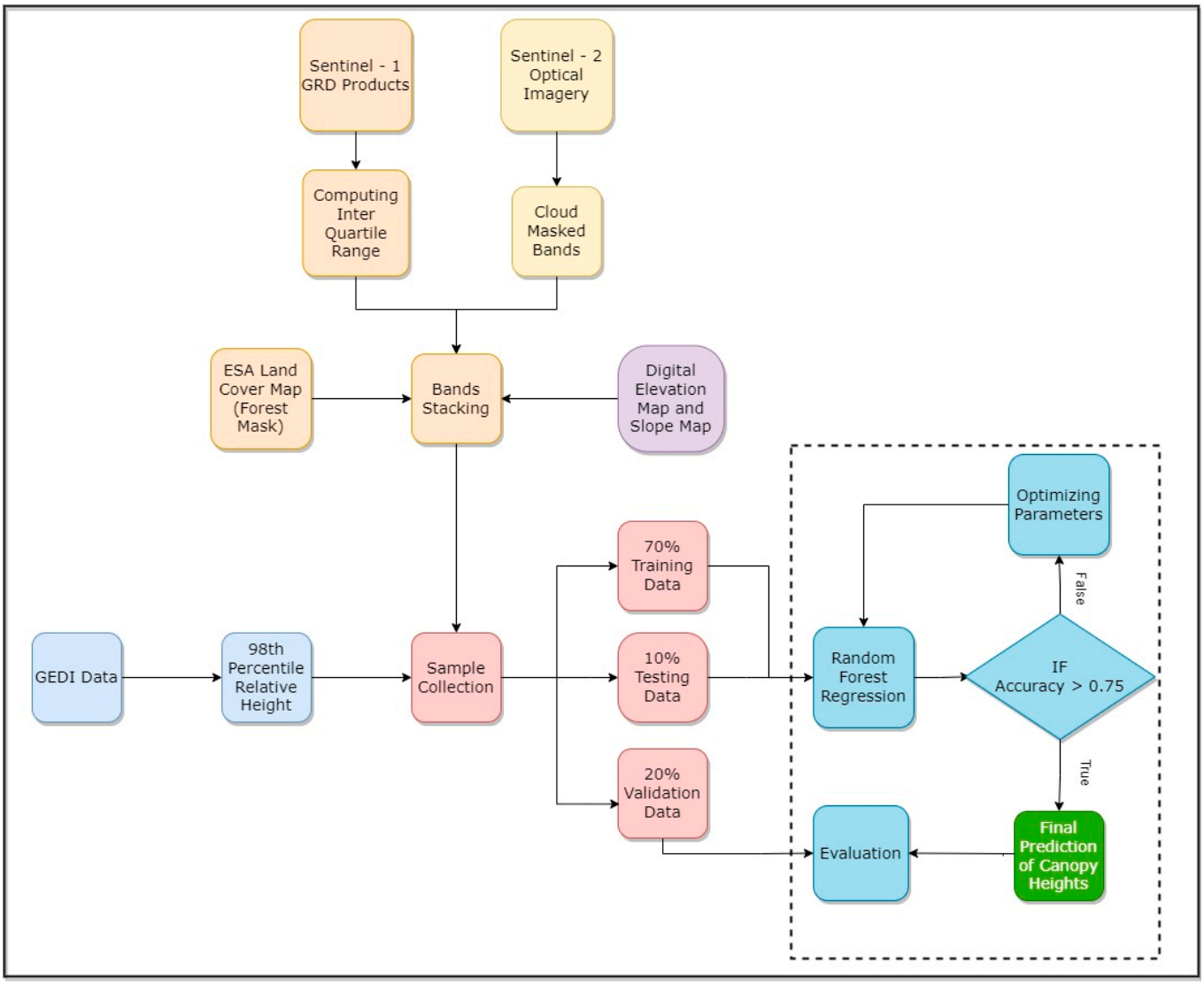

Figure 3. A flowchart of the machine learning-based canopy height estimation process.

We used the Jeffries Matusita-Spectral Angle Mapper (JMSAM) technique to collect spectral signatures of similar and dissimilar groups from the images. The analysis of hyperspectral imagery involves calculating the spectral angle between the reference spectra and the target spectra. The advantage of the SAM technique is that it compares the properties of the material in terms of spectral angles while being insensitive to illumination and shade. The Jeffries Matusita (JM) distance measure was used in combination with SAM to identify similar spectra. The average distance between two spectra is calculated by the JM distance. This method circumvents the modified divergence constraint by using an exponential factor that lends an exponentially diminishing weight to the growing separation between the spectra [53–55]. In order to identify similar spectra, we used the deterministic SAM along with the stochastic JM distance measure. This method considers the geometrical aspects (angle, distance) as well as the band information between the spectral vectors. The best match is therefore determined by the least separable distance between the spectral vectors at each band and the minor spectral angle between the vectors. A score map was generated with this method, with high and low values corresponding to the spectral signatures' similarity. Then, we used K-means clustering to extract the profiles into three groups: similar, dissimilar, and noisy profiles.

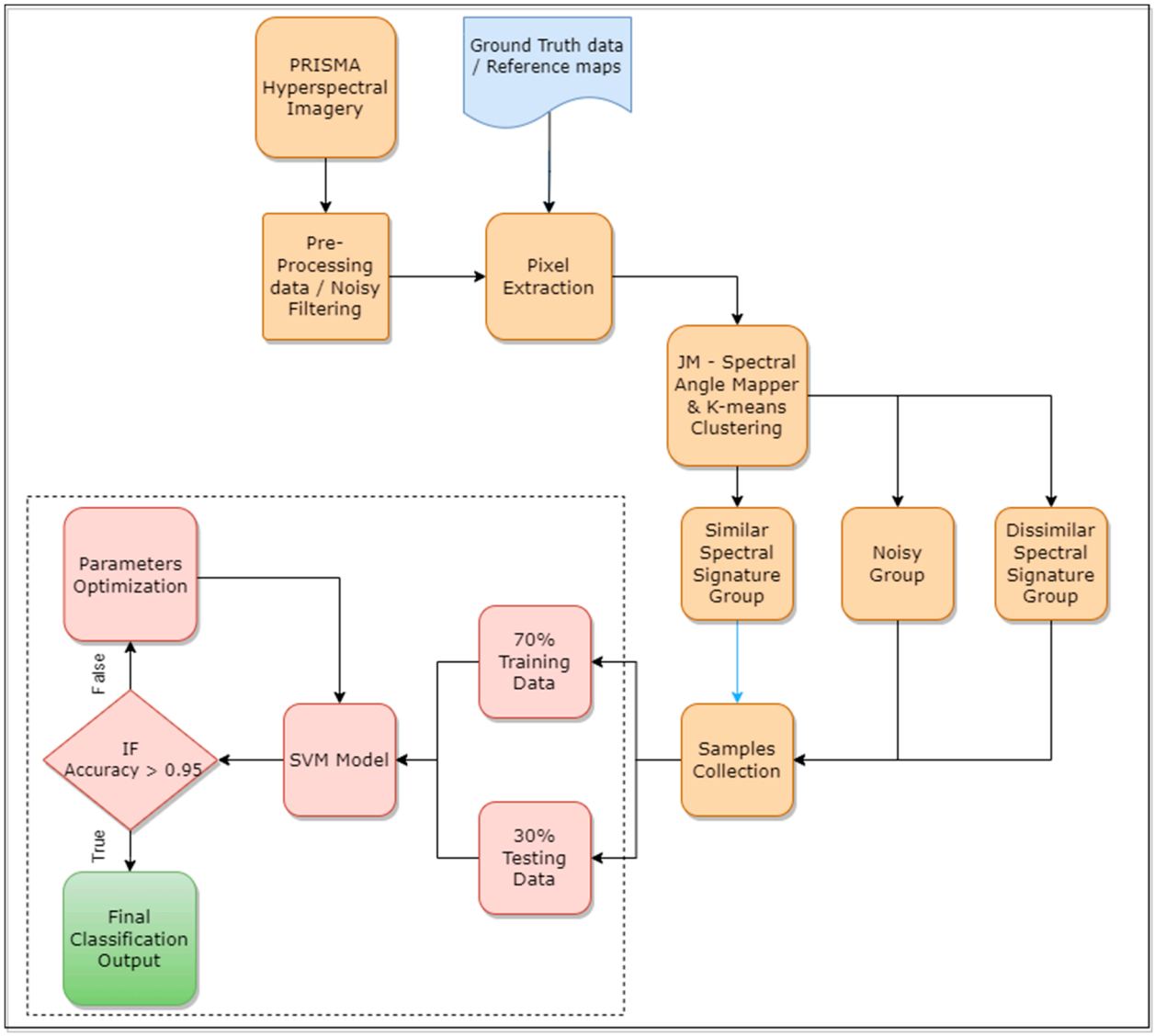

Figure 4. Stepwise flowchart of machine learning-based vegetation classification using PRISMA hyperspectral imagery.

A variety of supervised image-based land cover classification algorithms are available, such as support vector machine (SVM), random forest (RF), and K-nearest neighbour (KNN) [56]. For the present study, we trained the support vector machine classification model with a radial basis function (RBF) due to its high accuracy and a great generalization, irrespective of the sample size of the dataset. The model works on the structural risk-minimization principle and statistical learning theory. The optimal separating hyperplane with a maximum margin between the classes was found using the model with the training samples that are located at the edge of the class distribution [57–59]. Initially, we tried hyperparameter optimization to find the optimal values. However, this led to overfitting of the model, so instead, a Bayesian optimization technique was used. Then, we computed posterior probabilities using a trained SVM model by training the parameters with an additional sigmoid function to map outputs as probabilities. These posterior probabilities play an essential role in making an overall decision when the classifier is limited to making a small part of an overall decision.

For each vegetation type, we created a dataset of 500 samples in which 300 samples were collected from the similar-spectral-signatures group and labeled as 1 and another set of 200 samples were from dissimilar and noisy-spectral-signatures groups and labeled as 0.

These samples were divided into training and testing datasets with 70% and 30% of the total samples, respectively, and the SVM posterior probability model was trained using the training dataset. Then, K-fold cross-validation with K = 10 was performed to train the model with minimal error. The trained SVM model showed a testing accuracy of >0.95 for each class when testing with each class's respective testing dataset.

3.3. Extraction of Tree Canopy Temperatures from MODIS LST Product

Many thermal infrared imageries are available online, such as Landsat, Meteosat, Sentinel, Copernicus Global Land Service, etc., and they all have their limitations, as they either require multiple-step processing for them to be used as LST or have high temporal resolution. MODIS LST products, on the other hand, are readily available with no preprocessing needed and have a temporal resolution of one day. These products can be easily imported and worked on in the Google Earth Engine (GEE) API platform. As the classification obtained in this study was during the month of October 2021, all images from the same month were taken for consideration. To obtain a complete profile of the tree canopy temperature of the study area, the mean for all LST images was computed on GEE. The spatial resolution of the MODIS LST product was originally 1 km, and those of the canopy height and the LULC map are 30 m. For the purpose of analysis, we resampled the spatial resolution of the tree canopy temperature to a 30 m spatial resolution using an inverse distance weighted interpolation technique in ArcMap.

4. Results

4.1. LULC Classification Map

As per the methodology described in Section 3.2, we have mapped 12 different vegetation classes, as shown in Figure 5, excluding bare soil, unclassified vegetation, urban areas, and water. Details of each class are shown in Table 2. Significant classes of vegetation in this region of interest are class 5, class 8, class 2, class 4, and class 6, which represent coniferous trees, Euphorbia dendroides, evergreen oak, silicicole, and junipers, respectively. Coniferous trees and Euphorbia dendroides have coverages of 29% and 25%, respectively, whereas the remaining three classes have the least coverage area, around 2% each.

Table 2. Various Classes of Land Use, Land Cover Map.

Class Number	Class
−1	all other classifications
1	Holm oak
2	evergreen oak
3	olive
4	silicicole
5	coniferous trees
6	junipers
7	calicotome
8	Euphorbia dendroides
9	calicole
10	Mediterranean meadows
11	riparian forest
12	cork oak trees

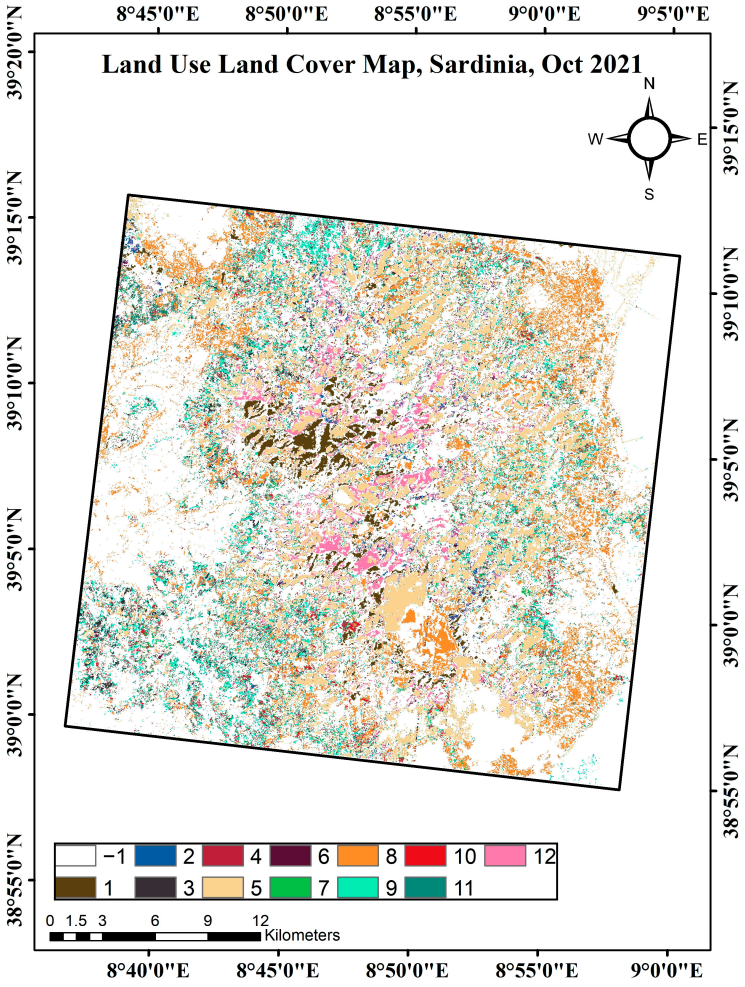

Figure 5. Land use, land cover map of Sardinia—the meaning of each color in the legend is stated in Table 2.

4.2. Canopy Height Map

For canopy height estimation, a random forest model was used, which has been run on Google Earth Engine (GEE). We trained this model with various variables (as mentioned in Section 3) to predict the canopy heights. Performance of this model was optimized by varying the number-of-trees parameter. This model successfully predicted the heights with an RMSE of 2.9176 m and an R^2 value of 0.791, which were obtained upon testing with the testing dataset of 1500 samples. The canopy height map is shown in Figure 6 and the model performance statistics can be seen in Figure 7, which shows the predicted vs. observed values for the canopy heights. Figure 7 also shows the final regression equation used for the model as an inset.

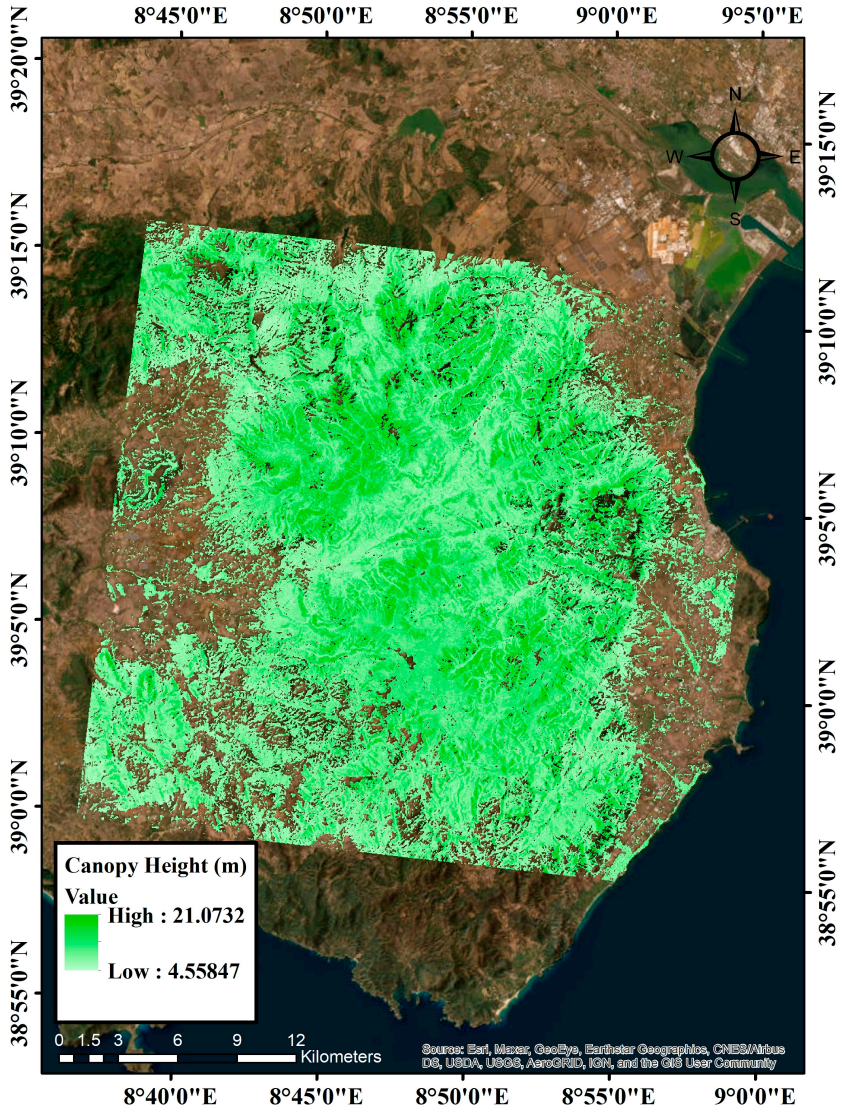

Figure 6. Canopy height map for canopy higher than 4.5 m. Darker green means higher canopy height.

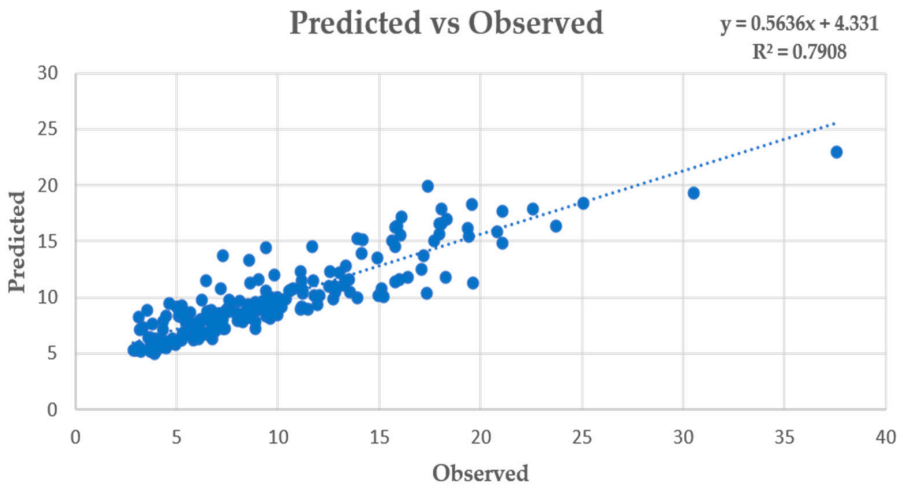

Figure 7. Random forest regression, predicted canopy heights vs. observed values from GEDI.

Furthermore, we continued the validation by comparing our results with the LULC map and observed that canopy heights that are less than 4.5 m were not predicted, since the minimum canopy height of GEDI's RH98 product for our region of interest is 4.5 m. By correlating the canopy height map with the classification map, we observed that only five classes, viz., evergreen oak, olive, junipers, silicicole, and riparian trees, were predicted for canopy heights. The canopy heights of these five classes were in the range of 4.5 m to 21 m, as shown in Figure 6. These images were exported as GeoTiff files for further analysis with canopy temperature map in ArcMap, as shown in Figure 8.

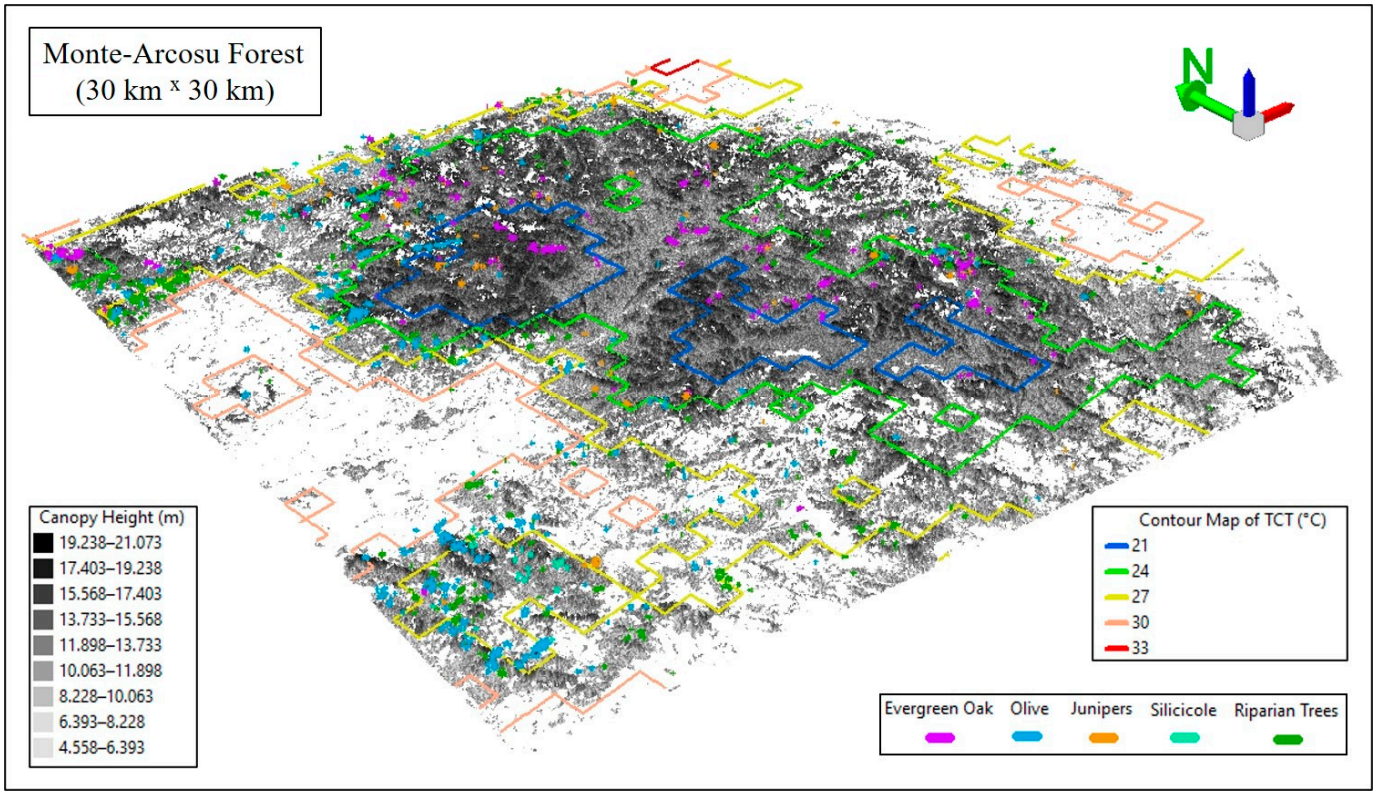

Figure 8. A 3D visualization of canopy heights, vegetation types, and canopy temperatures as contour lines.

4.3. Validation of LULC Classification and Canopy Height Maps

The main goal of this paper is to examine the relationship between the canopy heights of various vegetation classes and their corresponding tree canopy temperatures. We started the procedure in a stepwise manner, i.e., we initially classified the LULC types for the region of interest using hyperspectral imaging. The final classification map obtained with the SVM model has 12 classes, as shown in Figure 5 and Table 2.

The LULC map was validated using maps, viz., grassland maps, nature system maps, and a Corine land cover map, collected from various sources. In this study, we performed validation only for classes for which canopy heights were predicted, i.e., vegetation types of height greater than 4.5 m, and only these classes were used to study the tree canopy–temperature relationship. For each of these classes, 50 pixels were considered, and validation accuracy was calculated for them, which is the ratio of the correctly classified pixels to the total number of pixels considered. Along with the accuracy, a few other validation metrics, such as F1 score, recall, and precision, were also calculated, as shown in Table 3. These metrics allowed us to further assess the accuracy of the map. Precision and recall are helpful when the costs of false positive (FP) and false negative (FN) are different. F1 score is not intuitively easy to understand; however, it helps to assess when there is an uneven distribution of the classes. The accuracy of all the classes is greater than 80%, as

shown in Table 3. Given the absence of recent reference or ground truth data for validation, an uncertainty of up to ±5% inaccuracy can be anticipated. This classification map is a reference for the validation of the canopy heights map.

Table 3. Validation Metrics, Correlation Coefficients, and Mean Tree Canopy Temperatures for Different Tree Types.

S. No	Class	Accuracy (%)	Precision	Recall	F1 Score
1	evergreen oak	86	0.83	0.86	0.85
2	olive	80	0.85	0.72	0.78
3	juniper	86	0.86	0.86	0.86
4	silicicole	90	0.86	0.90	0.94
5	riparian trees	93	0.84	0.93	0.94

We then validated the canopy height estimations using the GEDI canopy height product as the ground truth. The trained random forest regression model was validated with a validation dataset of 3000 samples and obtained an RMSE of 3.63 m. We found this validation result reasonable and proceeded with the correlation analysis.

4.4. Tree Canopy Temperature and Its Relationship with Canopy Heights of Different Vegetation

MODIS surface temperature images for the entire month of October 2021 were collected, and the mean tree canopy temperature was computed over the region of interest in GEE, shown in Figure 9. Like the canopy heights, we extracted the mean tree canopy temperature for the five vegetation types, which are evergreen oak (23.21 °C), olive (23.93 °C), juniper (23.39 °C), silicicole (24.03 °C), and riparian trees (24.89 °C). These extracted values of canopy heights and temperatures for five different vegetation types were plotted against each other to check for any existing relationships between them, as shown in Figure 10. The following subsections for each class describe the inferences and correlations obtained for each of the plots.

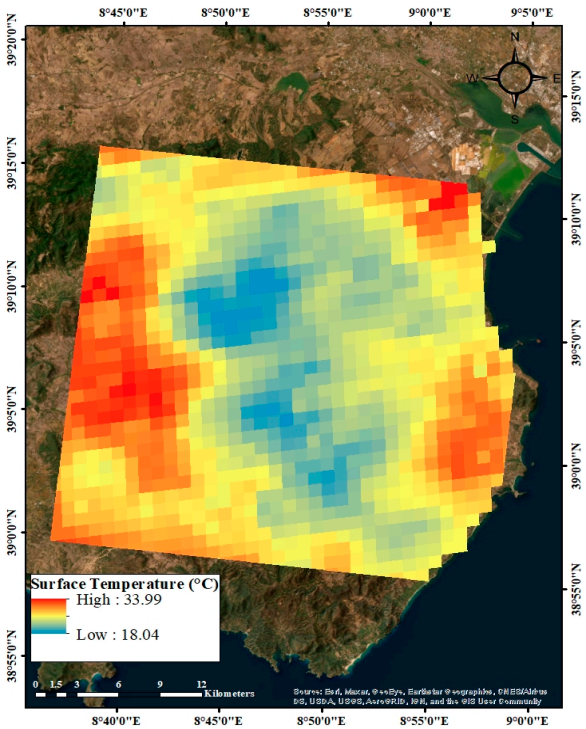

Figure 9. Tree canopy temperature map, October 2021.

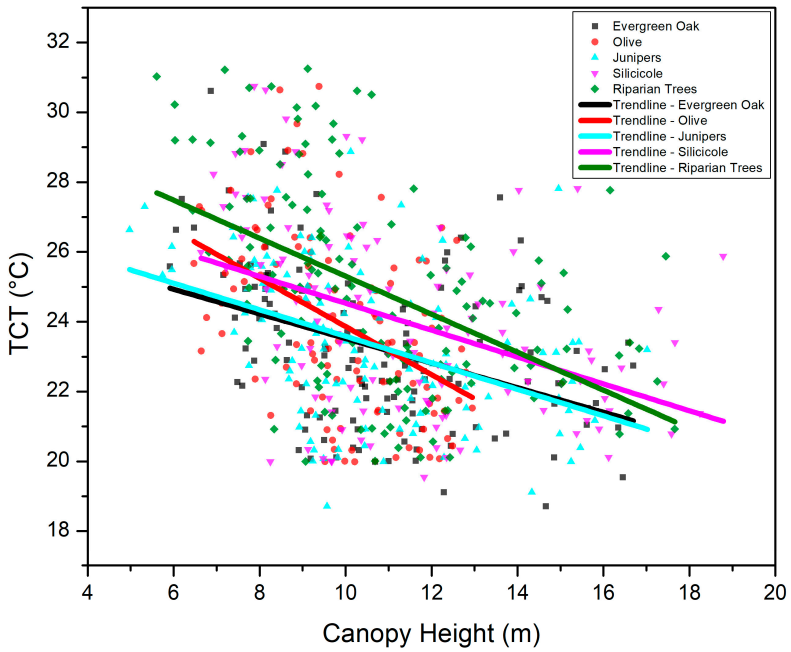

Figure 10. Scatter plot of tree canopy temperature (TCT) vs. canopy height for the five prevailing vegetation types (evergreen oak trees, olive trees, junipers, silicicole, and riparian trees) in the study area.

Vegetation Types

Evergreen oak trees: Figure 10 shows the scatter plot of tree canopy temperature against canopy height for evergreen oak trees. This vegetation type covered an area of 2% of our selected region of interest. The height of this class ranges from 6 m to 17 m and its corresponding tree canopy temperature ranges from 19 °C to 31 °C. A direct visual inspection of the plot shows that there is a decreasing trend between these variables, i.e., as the canopy height is increasing, there is an observed decrease in the canopy temperature of the tree. The trendline shown in the scatter plot has a slope of −0.35, which is seen as gentle slope, i.e., we only see a small decrease in canopy temperature when there is a significant increase in the canopy height. To further confirm the negative relationship between temperature and height, a correlation test was conducted between the canopy temperature and the canopy height. The result was as expected, showing a negative correlation between tree canopy temperature and canopy height, i.e., as one of the metrics increases, the other one decreases, and vice versa. The correlation coefficient obtained for evergreen oak is −0.41.

Olive trees: The scatter plot for olive trees is shown in Figure 10. The predicted canopy height for this type of vegetation ranged from 6.5 m to 13 m and the canopy temperature ranged from 20 °C to 31 °C. This class occupied a total of 4.1% of the study area. The following scatter plot also shows a linear trendline between the two metrics. Of all the other classes for which the analysis was carried out, olive trees showed the steepest slope, −0.69. The correlation test between the canopy temperature and the canopy height resulted in a negative coefficient, with a value of −0.45. This indicates that metrics are moderately correlated.

Junipers: Then, we analyzed junipers, for which the obtained scatter plot is shown in Figure 10. Canopy heights for this class varied from 4 m to 17 m and the tree canopy temperature ranged from 19 °C to 29 °C. In total, 2% of the ROI area was covered by junipers. Similarly to previous vegetation types, a linear trendline was obtained as shown in Figure 10, which has a slope value of −0.38. This value shows a less steep trendline, representing that the decrease in canopy temperature with the increase in canopy height is

comparatively small. The correlation test between these two metrics resulted in a coefficient value of −0.43, which, again, points towards moderately correlated metrics.

Silicicole: The silicicole family of trees ranged in height from 6.6 m to 19 m and canopy temperature varied from 19.5 °C to 31 °C. The scatter plot of this class is shown in Figure 10. The linear trendline shown in the figure has a slope of −0.38. The trees covered 2% of the ROI area. The correlation test conducted for the tree canopy temperature and canopy height for this class showed a negative correlation, with a coefficient value of −0.42.

Riparian trees: Finally, we analyzed riparian forest, and the scatter plot for it is shown in Figure 10. This vegetation type ranged from 6 m to 18 m in canopy height and from 20 °C to 31 °C in canopy temperature. The trendline for this class has a slope of −0.54, indicating a moderately steep slope. This represents that the change in canopy temperature is comparatively higher, with a slight change in temperature. The correlation test revealed a negative correlation coefficient of −0.50, showing moderately correlated metrics. However, this is the highest correlation coefficient among all vegetation classes that we analyzed.

A possible explanation for the inverse relationship that we found between canopy height and tree canopy temperature is the net cooling effect of evapotranspiration in the forest. During evapotranspiration, water is taken up by plant roots and transported to the leaves, where it is released into the air through stomata. As water evaporates from the leaves, it absorbs heat from the surrounding environment, which cools the plant and the surrounding area. The temperature of the surrounding air and the amount of radiation received from the sun can vary with height, which can affect the temperature of the leaves and the overall temperature of the canopy. The structure and density of the canopy can also affect its temperature, as a more open canopy allows for more air flow and convection, which can help to cool the leaves and to reduce the overall temperature of the canopy [60]. As the canopy height increases, the net radiation and sensible heat flux decrease, while the latent heat flux remains relatively constant. This results in an increased net cooling effect, which may explain the inverse relationship between canopy height and tree canopy temperature [1].

5. Conclusions and Discussion

From this study, we demonstrated the relationship between tree canopy temperature, canopy height, and vegetation type. This analysis was conducted for the southern part of Sardinia Island constituting the Monte-Arcosu Forest. As a part of this study, we created a canopy height map, a land use, land cover (LULC) map, and a canopy temperature map as the results of our analysis. Firstly, we estimated canopy heights using a random forest regression model on Sentinel-1 SAR data, Sentinel-2 multispectral data, and SRTM elevation and slope data as independent variables and canopy height measurements from the GEDI sensor as the dependent variable. Our model predicted canopy heights with an R^2 value of 0.791; however, it failed to predict canopy heights less than 4.5 m due to the limitation of the dependent variable (GEDI canopy height measurements). Secondly, we mapped LULC types using an SVM classifier with datasets of PRISMA hyperspectral bands as independent variables and labeled them using three different sources, namely, a national system map, a grasslands map, and a Copernicus land cover map. We were able to classify 12 different classes with an accuracy of greater than 80% for each class. Due to limitations of the canopy height estimation map, we considered only five classes, namely, evergreen oak, olive, junipers, silicicole, and riparian trees. Then, we extracted canopy temperatures for these five classes using the MODIS LST and the emissivity product. Since this product is available at a spatial resolution of 1 km, we resampled it to 30 m in order to compare it with our other results.

Using these three maps, we analyzed the relationship between canopy height and tree canopy temperature for each vegetation type in a scatter plot. All vegetation types showed a negative correlation and an inverse relationship between canopy height and tree canopy temperature. It is worth noting that the exact relationship between canopy height and temperature can vary depending on the specific environmental conditions and the type of

vegetation. While evapotranspiration can have a cooling effect on the surrounding area, other factors such as solar radiation, wind, and humidity can also play a role in determining the temperature of the canopy [61]. Further research is needed to fully understand the complex relationship between canopy height, evapotranspiration, and temperature. We would like to extend this study in more detail and to different regions to improve the understanding of the relationship between forest canopy height and canopy temperature to better understanding the local forest climate.

This study can be improved using field-surveyed canopy height measurements of all heights or other higher-resolution canopy height data, as we only used the relatively low-resolution, remotely sensed GEDI data. Furthermore, using canopy temperature data with a higher spatial resolution than 1 km would enable a more detailed analysis and results. We only used readily and freely available data for our study.

Author Contributions: Conceptualization, R.U.S. and S.B.J.; methodology, R.U.S. and S.B.J.; software, R.U.S. and S.B.J.; validation, R.U.S., S.B.J. and K.D.; formal analysis, R.U.S., S.B.J. and K.D.; investigation, R.U.S. and K.D.; resources, R.U.S.; data curation, R.U.S. and S.B.J.; writing—original draft preparation, R.U.S. and S.B.J.; writing—review and editing, R.U.S., S.B.J. and K.D.; visualization, R.U.S., S.B.J. and K.D.; supervision, R.U.S. and K.D.; project administration, R.U.S.; funding acquisition, R.U.S. All authors have read and agreed to the published version of the manuscript.

Funding: This research received no external funding.

Data Availability Statement: PRISMA imagery that support the findings of this study are accessed from Italian Space Agency's (http://prisma.asi.it/) after the registration (ID: ITA_ScN1_0542_2$).

Acknowledgments: Authors would like to thank the EOSIAL Lab at the School of Aerospace Engineering for their support in carrying out this research.

Conflicts of Interest: The authors declare no conflict of interest.

References

1. Zhang, Z.; Li, X.; Liu, H. Biophysical feedback of forest canopy height on land surface temperature over contiguous United States. *Environ. Res. Lett.* **2022**, *17*, 34002. [CrossRef]
2. Hulley, G.C.; Ghent, D.; Göttsche, F.M.; Guillevic, P.C.; Mildrexler, D.J.; Coll, C. Land Surface Temperature. In *Taking the Temperature of the Earth*; Elsevier BV: Amsterdam, The Netherlands, 2019; pp. 57–127.
3. Li, Z.-L.; Duan, S.-B. Land Surface Temperature. *Compr. Remote Sens.* **2018**, *1–9*, 264–283. [CrossRef]
4. Kustas, W.; Anderson, M. Advances in thermal infrared remote sensing for land surface modeling. *Agric. For. Meteorol.* **2009**, *149*, 2071–2081. [CrossRef]
5. Teufel, B.; Sushama, L.; Poitras, V.; Dukhan, T.; Bélair, S.; Miranda-Moreno, L.; Sun, L.; Sasmito, A.; Bitsuamlak, G. Impact of COVID-19-Related Traffic Slowdown on Urban Heat Characteristics. *Atmosphere* **2021**, *12*, 243. [CrossRef]
6. Jallu, S.B.; Shaik, R.U.; Srivastav, R.; Pignatta, G. Assessing the effect of COVID-19 lockdown on surface urban heat island for different land use/cover types using remote sensing. *Energy Nexus* **2022**, *5*, 100056. [CrossRef]
7. Chuvieco, E.; Cocero, D.; Riaño, D.; Martin, P.; Martínez-Vega, J.; de la Riva, J.; Pérez, F. Combining NDVI and surface temperature for the estimation of live fuel moisture content in forest fire danger rating. *Remote Sens. Environ.* **2004**, *92*, 322–331. [CrossRef]
8. Escuin, S.; Navarro, R.; Fernández, P. Fire severity assessment by using NBR (Normalized Burn Ratio) and NDVI (Normalized Difference Vegetation Index) derived from LANDSAT TM/ETM images. *Int. J. Remote Sens.* **2008**, *29*, 1053–1073. [CrossRef]
9. Kuenzer, C.; Dech, S. (Eds.) *Thermal Infrared Remote Sensing*; Springer: Dordrecht, The Netherlands, 2013; Volume 17. [CrossRef]
10. Vlassova, L.; Pérez-Cabello, F.; Mimbrero, M.R.; Llovería, R.M.; García-Martín, A. Analysis of the Relationship between Land Surface Temperature and Wildfire Severity in a Series of Landsat Images. *Remote Sens.* **2014**, *6*, 6136–6162. [CrossRef]
11. Roy, B.; Bari, E. Examining the relationship between land surface temperature and landscape features using spectral indices with Google Earth Engine. *Heliyon* **2022**, *8*, e10668. [CrossRef]
12. Tao, S.; Guo, Q.; Li, C.; Wang, Z.; Fang, J. Global patterns and determinants of forest canopy height. *Ecology* **2016**, *97*, 3265–3270. [CrossRef]
13. Xu, P.; Zhou, T.; Zhao, X.; Luo, H.; Gao, S.; Li, Z.; Cao, L. Diverse responses of different structured forest to drought in Southwest China through remotely sensed data. *Int. J. Appl. Earth Obs. Geoinf.* **2018**, *69*, 217–225. [CrossRef]
14. Zakrzewska, A.; Kopeć, D.; Ochtyra, A.; Potůčková, M. Can canopy temperature acquired from an airborne level be a tree health indicator in an urban environment? *Urban For. Urban Green.* **2023**, *79*, 127807. [CrossRef]
15. Gross, G. Effects of different vegetation on temperature in an urban building environment. Micro-scale numerical experiments. *Meteorol. Z.* **2012**, *21*, 399–412. [CrossRef]

16. Helletsgruber, C.; Gillner, S.; Gulyás, Á.; Junker, R.R.; Tanács, E.; Hof, A. Identifying Tree Traits for Cooling Urban Heat Islands—A Cross-City Empirical Analysis. *Forests* **2020**, *11*, 1064. [CrossRef]
17. Kumar, S.; Kumar, A. Hotspot and trend analysis of forest fires and its relation to climatic factors in the western Himalayas. *Nat. Hazards* **2022**, *114*, 3529–3544. [CrossRef]
18. Chaparro, D.; Vall-Llossera, M.; Piles, M.; Camps, A.; Rudiger, C.; Riera-Tatche, R. Predicting the Extent of Wildfires Using Remotely Sensed Soil Moisture and Temperature Trends. *IEEE J. Sel. Top. Appl. Earth Obs. Remote Sens.* **2016**, *9*, 2818–2829. [CrossRef]
19. Littell, J.S.; Peterson, D.L.; Riley, K.L.; Liu, Y.; Luce, C.H. A review of the relationships between drought and forest fire in the United States. In *Global Change Biology*; Blackwell Publishing Ltd.: Hoboken, NJ, USA, 2016; Volume 22, pp. 2353–2369. [CrossRef]
20. Brovkin, V.; Sitch, S.; Von Bloh, W.; Claussen, M.; Bauer, E.; Cramer, W. Role of land cover changes for atmospheric CO_2 increase and climate change during the last 150 years. *Glob. Chang. Biol.* **2004**, *10*, 1253–1266. [CrossRef]
21. Liao, W.; Liu, X.; Burakowski, E.; Wang, D.; Wang, L.; Li, D. Sensitivities and Responses of Land Surface Temperature to Deforestation-Induced Biophysical Changes in Two Global Earth System Models. *J. Clim.* **2020**, *33*, 8381–8399. [CrossRef]
22. Pielke, R.A. Land Use and Climate Change. *Science* **2005**, *310*, 1625–1626. [CrossRef]
23. Sh, S. Application of Geographic Information System (GIS) in Forest Management. *J. Geogr. Nat. Disasters* **2015**, *5*, 1000145. [CrossRef]
24. Venkata, K.M.; Yelisetty, N. Use of Geo-spatial database in Sustainable Forest Management. In Proceedings of the International Archives of the Photogrammetry, Remote Sensing and Spatial Information Sciences, Goa, India, 27–30 September 2006. [CrossRef]
25. Næsset, E. Predicting forest stand characteristics with airborne scanning laser using a practical two-stage procedure and field data. *Remote Sens. Environ.* **2002**, *80*, 88–99. [CrossRef]
26. Allen, C.D.; Breshears, D.D.; McDowell, N.G. On underestimation of global vulnerability to tree mortality and forest die-off from hotter drought in the Anthropocene. *Ecosphere* **2015**, *6*, 1–55. [CrossRef]
27. Au, T.F.; Maxwell, J.T.; Robeson, S.M.; Li, J.; Siani, S.M.O.; Novick, K.A.; Dannenberg, M.P.; Phillips, R.P.; Li, T.; Chen, Z.; et al. Younger trees in the upper canopy are more sensitive but also more resilient to drought. *Nat. Clim. Chang.* **2022**, *12*, 1168–1174. [CrossRef]
28. Stovall, A.E.L.; Shugart, H.; Yang, X. Tree height explains mortality risk during an intense drought. *Nat. Commun.* **2019**, *10*, 4385. [CrossRef]
29. Coops, N.C.; Tompalski, P.; Goodbody, T.R.; Queinnec, M.; Luther, J.E.; Bolton, D.K.; White, J.C.; Wulder, M.A.; van Lier, O.R.; Hermosilla, T. Modelling lidar-derived estimates of forest attributes over space and time: A review of approaches and future trends. *Remote. Sens. Environ.* **2021**, *260*, 112477. [CrossRef]
30. Potapov, P.; Li, X.; Hernandez-Serna, A.; Tyukavina, A.; Hansen, M.C.; Kommareddy, A.; Pickens, A.; Turubanova, S.; Tang, H.; Silva, C.E.; et al. Mapping global forest canopy height through integration of GEDI and Landsat data. *Remote. Sens. Environ.* **2021**, *253*, 112165. [CrossRef]
31. Meng, P.; Wang, H.; Qin, S.; Li, X.; Song, Z.; Wang, Y.; Yang, Y.; Gao, J. Health assessment of plantations based on LiDAR canopy spatial structure parameters. *Int. J. Digit. Earth* **2022**, *15*, 712–729. [CrossRef]
32. LeBlon, B.; Bourgeau-Chavez, L.; San-Miguel-Ayanz, J. Use of Remote Sensing in Wildfire Management. In *Sustainable Development—Authoritative and Leading Edge Content for Environmental Management*; Curkovic, S., Ed.; InTech Press: Rijeka, Croatia, 2012; pp. 55–82.
33. Choi, C.; Cazcarra-Bes, V.; Guliaev, R.; Pardini, M.; Papathanassiou, K.P.; Qi, W.; Armston, J.; Dubayah, R. Large Scale Forest Height Mapping by Combining TanDEM-X and GEDI Data. *IEEE J. Sel. Top. Appl. Earth Obs. Remote Sens.* **2023**, *16*, 2374–2385. [CrossRef]
34. LaRue, E.A.; Fahey, R.T.; Alveshere, B.C.; Atkins, J.W.; Bhatt, P.; Buma, B.; Chen, A.; Cousins, S.; Elliott, J.M.; Elmore, A.J.; et al. A theoretical framework for the ecological role of three-dimensional structural diversity. *Front. Ecol. Environ.* **2023**, *21*, 4–13. [CrossRef]
35. Lang, N.; Schindler, K.; Wegner, J.D. Country-wide high-resolution vegetation height mapping with Sentinel-2. *Remote Sens. Environ.* **2019**, *233*, 111347. [CrossRef]
36. Liu, X.; Su, Y.; Hu, T.; Yang, Q.; Liu, B.; Deng, Y.; Tang, H.; Tang, Z.; Fang, J.; Guo, Q. Neural network guided interpolation for mapping canopy height of China's forests by integrating GEDI and ICESat-2 data. *Remote Sens. Environ.* **2022**, *269*, 112844. [CrossRef]
37. Pielke, R.A.; Pitman, A.; Niyogi, D.; Mahmood, R.; McAlpine, C.; Hossain, F.; Goldewijk, K.K.; Nair, U.; Betts, R.; Fall, S.; et al. Land use/land cover changes and climate: Modeling analysis and observational evidence. *Wiley Interdiscip. Rev. Clim. Change* **2011**, *2*, 828–850. [CrossRef]
38. Cao, Q.; Wu, J.; Yu, D.; Wang, W. The biophysical effects of the vegetation restoration program on regional climate metrics in the Loess Plateau, China. *Agric. For. Meteorol.* **2019**, *268*, 169–180. [CrossRef]
39. Abera, T.A.; Heiskanen, J.; Pellikka, P.; Rautiainen, M.; Maeda, E.E. Clarifying the role of radiative mechanisms in the spatiotemporal changes of land surface temperature across the Horn of Africa. *Remote Sens. Environ.* **2019**, *221*, 210–224. [CrossRef]
40. Christiansen, D.M.; Iversen, L.L.; Ehrlén, J.; Hylander, K. Changes in forest structure drive temperature preferences of boreal understorey plant communities. *J. Ecol.* **2022**, *110*, 631–643. [CrossRef]

41. Hasnat, G.N.T. A Time Series Analysis of Forest Cover and Land Surface Temperature Change Over Dudpukuria-Dhopachari Wildlife Sanctuary Using Landsat Imagery. *Front. For. Glob. Chang.* **2021**, *4*, 687988. [CrossRef]
42. Zhang, Y.; Liang, S. Impacts of land cover transitions on surface temperature in China based on satellite observations. *Environ. Res. Lett.* **2018**, *13*, 24010. [CrossRef]
43. Lam, N.S.-N. Methodologies for Mapping Land Cover/Land Use and its Change. In *Advances in Land Remote Sensing: System, Modeling, Inversion and Application*; Liang, S., Ed.; Springer: Dordrecht, The Netherlands, 2008; pp. 341–367. [CrossRef]
44. Rozario, P.F.; Oduor, P.; Kotchman, L.; Kangas, M. Transition Modeling of Land-Use Dynamics in the Pipestem Creek, North Dakota, USA. *J. Geosci. Environ. Prot.* **2017**, *05*, 182–201. [CrossRef]
45. Vivone, G. Multispectral and hyperspectral image fusion in remote sensing: A survey. *Inf. Fusion* **2023**, *89*, 405–417. [CrossRef]
46. Liu, N.; Townsend, P.A.; Naber, M.R.; Bethke, P.C.; Hills, W.B.; Wang, Y. Hyperspectral imagery to monitor crop nutrient status within and across growing seasons. *Remote Sens. Environ.* **2021**, *255*, 112303. [CrossRef]
47. Shaik, R.U.; Laneve, G.; Fusilli, L. An Automatic Procedure for Forest Fire Fuel Mapping Using Hyperspectral (PRISMA) Imagery: A Semi-Supervised Classification Approach. *Remote Sens.* **2022**, *14*, 1264. [CrossRef]
48. Shaik, R.U.; Periasamy, S.; Zeng, W. Potential Assessment of PRISMA Hyperspectral Imagery for Remote Sensing Applications. *Remote Sens.* **2023**, *15*, 1378. [CrossRef]
49. Salis, M.; Ager, A.A.; Alcasena, F.J.; Arca, B.; Finney, M.A.; Pellizzaro, G.; Spano, D. Analyzing seasonal patterns of wildfire exposure factors in Sardinia, Italy. *Environ. Monit. Assess.* **2014**, *187*, 1–20. [CrossRef] [PubMed]
50. Santarsiero, V. A Remote Sensing Methodology to Assess the Abandoned Arable Land Using NDVI Index in Basilicata Region. In Proceedings of the Computational Science and Its Applications–ICCSA 2021, Cagliari, Italy, 13–16 September 2021; pp. 695–703.
51. Tucci, B.; Nolè, G.; Lanorte, A.; Santarsiero, V.; Cillis, G.; Scorza, F.; Murgante, B. Assessment and Monitoring of Soil Erosion Risk and Land Degradation in Arable Land Combining Remote Sensing Methodologies and RUSLE Factors. In *Information for a Better World: Shaping the Global Future*; Springer Science and Business Media LLC: Berlin/Heidelberg, Germany, 2021; pp. 704–716. [CrossRef]
52. Büttner, G. CORINE Land Cover and Land Cover Change Products. In *Land Use and Land Cover Mapping in Europe*; Manakos, I., Braun, M., Eds.; Springer Science and Business Media LLC: Dordrecht, Switzerland, 2014; Volume 18, pp. 55–74.
53. Chang, C.-C.; Du, Y.; Ren, H.; Jensen, J.O.; D'Amico, F.M. New hyperspectral discrimination measure for spectral characterization. *Opt. Eng.* **2004**, *43*, 1777–1786. [CrossRef]
54. Laliberte, A.; Browning, D.; Rango, A. A comparison of three feature selection methods for object-based classification of sub-decimeter resolution UltraCam-L imagery. *Int. J. Appl. Earth Obs. Geoinf.* **2012**, *15*, 70–78. [CrossRef]
55. Vishnu, S.; Nidamanuri, R.R.; Bremananth, R. Spectral material mapping using hyperspectral imagery: A review of spectral matching and library search methods. *Geocarto Int.* **2013**, *28*, 171–190. [CrossRef]
56. Khatami, R.; Mountrakis, G.; Stehman, S.V. A meta-analysis of remote sensing research on supervised pixel-based land-cover image classification processes: General guidelines for practitioners and future research. *Remote Sens. Environ.* **2016**, *177*, 89–100. [CrossRef]
57. Guo, Y.; Yin, X.; Zhao, X.; Yang, D.; Bai, Y. Hyperspectral image classification with SVM and guided filter. *EURASIP J. Wirel. Commun. Netw.* **2019**, *2019*, 56. [CrossRef]
58. Thai, L.H.; Hai, T.S.; Thuy, N.T. Image Classification using Support Vector Machine and Artificial Neural Network. *Int. J. Inf. Technol. Comput. Sci.* **2012**, *4*, 32–38. [CrossRef]
59. Kang, X.; Li, S.; Benediktsson, J.A. Spectral–Spatial Hyperspectral Image Classification With Edge-Preserving Filtering. *IEEE Trans. Geosci. Remote Sens.* **2014**, *52*, 2666–2677. [CrossRef]
60. Still, C.J.; Rastogi, B.; Page, G.F.M.; Griffith, D.M.; Sibley, A.; Schulze, M.; Hawkins, L.; Pau, S.; Detto, M.; Helliker, B.R. Imaging canopy temperature: Shedding (thermal) light on ecosystem processes. *New Phytol.* **2021**, *230*, 1746–1753. [CrossRef] [PubMed]
61. Hou, M.; Tian, F.; Zhang, T.; Huang, M. Evaluation of canopy temperature depression, transpiration, and canopy greenness in relation to yield of soybean at reproductive stage based on remote sensing imagery. *Agric. Water Manag.* **2019**, *222*, 182–192. [CrossRef]